J. Text. Color. Polym. Sci., **Vol. 16**, No. 2, pp 113 -127 (2019)

Kinetics and thermodynamics of aniline blue adsorption onto cross-linked gelatin/chitosan polymer blends

Aly Okasha[a] *, H. S. Ghoneim[b], E. M. Khalil[b], S. K. Mohamed[b]

[a] Spectroscopy Department, Physics Division, National Research Centre, 33 El Bohouth Street, Dokki-Giza P.O. 12622, [b] Chemistry Department, Faculty of Science, Helwan University, Ain Helwan, Cairo, 11795, Egypt

FILMS of cross-linked gelatin/chitosan blends have been successfully synthesized using glutaraldehyde as a cross-linker. The synthesized samples were characterized using infrared Fourier transformation (FT-IR), and X-ray diffraction (XRD). The solubility in aqueous media, the pH- responsive swelling and point of zero surface charge were explored. The adsorption efficiency of samples for the removal of the anionic dye aniline blue from aqueous media has been studied. The parameters that affect the adsorption efficiency as pH, initial dye concentration, contact time and temperature have been examined. Kinetics studies showed that the adsorption process was well described by the pseudo-second-order model and the equilibrium adsorption results fitted Freundlich model. Fitting the experimental data with Dubinin-Radushkevich model indicated a predominant physisorption mechanism. The maximum dye removal achieved by 1:1 gelatin/chitosan at pH 5 and 35°C was 99.8%. The activation energy for the adsorption process increases as the chitosan content increases which indicating chemisorption behavior. Thermodynamic studies indicated that the adsorption is spontaneous, endothermic in nature and results in higher entropy.

Keywords: Adsorption, Gelatin, Chitosan, Kinetics, Thermodynamics

Introduction

Nowadays the water pollution is a worldwide problem due to economic and technological progress. One of the most serious water pollutants are dyes which are used with a large scale in many industries. The discharge of dye-contaminated wastewater has numerous impacts on the human, animals and plants. The ingestion, contact with external organs or inhalation of dyes results in serious health problems [1]. Synthetic dyes represent a serious threat to the environment and human due to their toxicity and non-biodegradability [2]. Aniline blue is a water-soluble synthetic dye that is employed in the textile industry for staining of cotton, nylon, silk, and wool. It is an acidic dye of triarylmethane category where a central carbon atom is attached to two benzene rings and one p-quinoid group. The removal of dyes from industrial wastewater is a necessity but costly from economic points of view. Several techniques have been employed to remove dyes from industrial wastewater as osmosis [3], coagulation [4], advanced oxidation processes [5], photo degradation[6], reverse membrane separation [7] and adsorption [8, 9]. Adsorption is considered as a fast, efficient and economic method compared to other methods, and it has been successfully employed for dye removal from industrial wastewater. The naturally occurring adsorbents as natural polymers are widely used in wastewater treatment because they are biodegradable, cheap, renewable, nontoxic and available materials [10]. Gelatin is a natural polymer obtained from the hydrolysis of collagen. Gelatin chains have both positively charged amino acids (arginine, lysine) and negatively charged amino acids (glutamate, aspartate) so it is characterized by hydrophobicity, biodegradability and high water-uptake. However, the low stability of gelatin in wet conditions and moderate temperature limits its uses as adsorbent [11]. Different modifications have been employed

* Corresponding author. E-mail: aliokasha2@yahoo.com

DOI: 10.21608/jtcps.2019.14878.1024

for gelatin to produce effective adsorbents for dyes such as cross-linking [12], blending with other polymers [13], blending with inorganic materials as bentonite [14], carbon nanotubes and iron oxide [11]. Chitosan is produced from the deacetylation of the natural polysaccharide chitin and it is characterized by its high hydrophobicity, non-toxicity and biodegradability [15]. Chitosan chains contain both amino ($–NH_2$) and hydroxyl (–OH) groups which makes it ideal for the removal of both negatively charged pollutants from aqueous solutions due to the positive charge on protonated amine groups. Chitosan dissolves in weak acids so chemical modifications such as cross-linking or grafting are employed to enhances its stability [16]. Researchers have extensively studied the removal of different dyes by chitosan [17], cross-linked chitosan [18], chitosan nanocomposite and chitosan blend with another polymer [13].

To the best of our knowledge, few researches were directed towards gelatin/chitosan blends as an adsorbent for wastewater treatment [13]. In this article, cross-linked gelatin and gelatin/chitosan blends have been synthesized using glutaraldehyde as a cross-linker and used for adsorption of aniline blue from aqueous media. To explore the structure and morphology of the synthesized samples FT-IR and XRD are used. The pH-responsive swelling and point of zero surface charge of the samples are explored. The stability of the samples against dissolution in aqueous solutions at different temperatures is investigated. The kinetics and isotherms of aniline blue adsorption onto the synthesized samples are investigated and used to calculate the activation energy of adsorption.

Experimental

Materials

Gelatin and glutaraldehyde were purchased from El Nasr Pharmaceutical Chemicals EDWIC, Egypt. Chitosan (M.M. 10,000–300,000) was supplied by Acros organics. Aniline blue (AB) was purchased from ALPHA, UK. All other chemicals were of analytical chemical grade and were used as received. The structure of Aniline blue (molecular formula is $C_{32}H_{25}N_3Na_2O_9S_3$ and molecular weight is 737.74) is illustrated in scheme 1.

Synthesis of cross-linked gelatin and gelatin/chitosan blends.

The polymer and polymer blends were prepared as films by the casting method. The cross-linked gelatin sample was prepared as follows: gelatin (6g) was added to 75 ml of distilled water and stirred at 40 ^{o}C till a homogeneous solution was obtained. Then, a solution of glutaraldehyde (0.3 ml) in 2% acetic acid (10 ml) was added drop by drop during stirring. The mixture was poured in a petri dish and left to dry at room temperature. For the synthesis of gelatin/chitosan blends, the same procedure was done. First, chitosan solution (definite weight of chitosan was dissolved in 2% acetic acid) was added to the gelatin solution and stirred for 30 min. Then glutaraldehyde solution (as 5 % v/w of glutaraldehyde to polymer) was added drop wise during stirring. In the casting process, the volume poured in the petri dish was controlled to get similar film thickness for all synthesized samples. The samples code and composition are mentioned in Table 1. All prepared samples were washed by distilled water to remove any unreacted polymers, cross-linker and acetic acid. Scheme 2 shows the expected chemical structure of glutaraldehyde Chitosan/Gelatin blend.

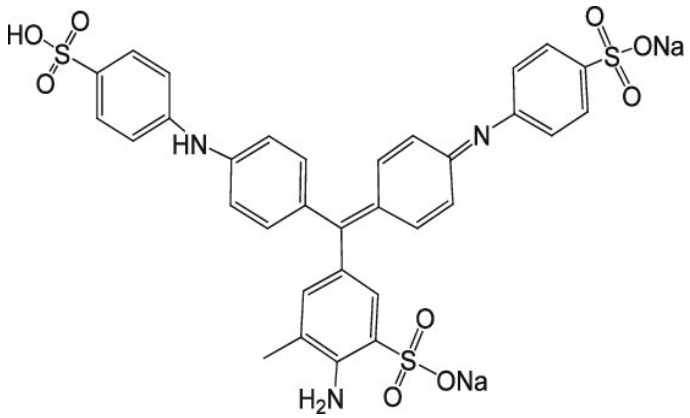

Scheme 1. Chemical structure of AB

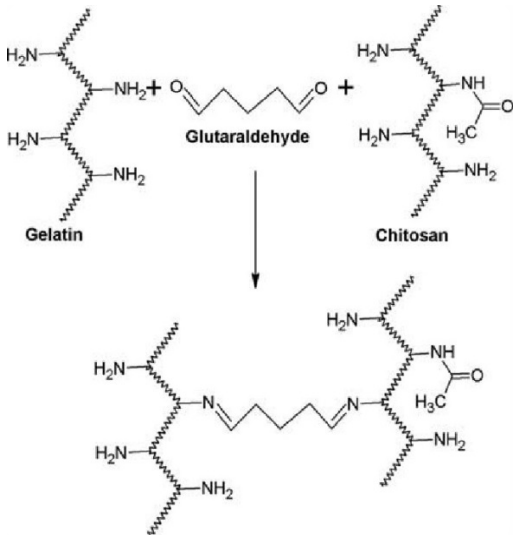

Scheme 2. The chemical structure of glutaraldehyde Chitosan/Gelatin blends.

TABLE 1 Samples codes and compositions.

Sample code	Gelatin (% wt)	Chitosan (% wt)
G100	100	-
G75	75	25
G50	50	50
G25	25	75

Characterization

Fourier transform infrared (FT-IR) spectra were recorded on FT-IR spectroscopy (FT-IR-6100 Jasco, Japan), using KBr pellets in the range of 4000–400 cm^{-1} at room temperature with spectral resolution 4 cm^{-1}. X–ray diffraction (XRD) studies were carried out using X–Ray Diffractometer (X'Pert Pro, PANanalytical, Netherlands) with Cu Kα radiation (λ = 0.15406 nm) in the 2θ range of 4º to 80º. For solubility studies, the solubility of the synthesized samples in aqueous media was checked by immersing 0.5 g of each sample in 100 ml distilled water for 24 h at different temperatures up to 50°C. Then, the samples were filtered and dried at room temperature till constant weight. The degree of solubility (%) of the samples was estimated by dividing the final weight by the initial weight × 100.

pH-responsive equilibrium swelling and point of zero surface charge.

The degree of equilibrium swelling (ES) of the samples was detected as follows: 0.1 g of each sample was immersed in 25 ml of different buffer solutions (2.0 - 9.0) and temperature 25°C for 24 hours to attain equilibrium. Swollen samples were collected and immediately weighed and the ES value of each sample was detected as follows:

$$ES = \frac{W_e - W_d}{W_d} \quad (1)$$

where W_d and W_e are the weight of dry and swollen samples at equilibrium respectively.

The point of zero surface charge is defined as the pH value at which net surface charge is zero and it is estimated by batch equilibrium method [19]. In this method, KNO_3 solution (0.1 M), is used as an inert electrolyte, and its initial pH (pH_i) was adjusted using 0.1 M HCl or NaOH solutions in a pH range of 2 –10. Briefly, a mixture of 0.1 g of each in 25 ml of KNO_3 solutions with definite pH_i was shaken at 298 K for 24 h then the final pH (pH_f) was measured. pH_{pzc} is the pH at which ($pH_i - pH_f$) = zero and it is detected from the plot of ($pH_i - pH_f$) versus pH_i.

Adsorption studies

For all adsorption experiments, adsorbate/ adsorbent mixtures were shaken for 24 hours to attain equilibrium. The dye solution concentration was detected using Agilant carry 100 spectrophotometer at a wavelength (λ_{max}) 610 nm where the dyes concentrations were detected on the calibration curve using Beer–Lambert law. The percentage of dye removal (%*E*) and the adsorption capacity, q_e (mg g^{-1}) were calculated as follows:

$$\%E = \frac{C_o - C_e}{C_o} * 100 \quad (2)$$

$$q_e = (C_o - C_e)\frac{V}{m} \quad (\text{mg g}^{-1}) \quad (3)$$

where C_o and C_e are the initial concentration and equilibrium concentration of the dye solution (mg L^{-1}), respectively. *V* is the volume of the dye solution (L) and m is the weight of adsorbent (g). The factors affecting E% and q_e such as pH (2-9), contact time, initial dye concentration (10, 20, 30, 50 and 100 mg L^{-1}) and temperature (20 - 40 °C) were investigated.

Adsorption Kinetics

In this study, 0.1 g of adsorbent (G100, G75, G50 or G25) was soaked in AB solution of initial concentration 30 mg L^{-1} at pH 5.0 and definite temperature (20 - 40°C). The mixtures were shaken and AB solution concentration was detected at different time intervals up to equilibrium (24 h).

Adsorption isotherms

In the adsorption isotherm studies, 0.1 g of adsorbent was soaked in AB solution with an initial concentration of 10, 20, 30, 50 and 100 mg L^{-1} at pH 5.0 and definite temperature (20, 25, 30, 35 °C).

Thermodynamics studies

In this study, 0.1 g of each sample was soaked in ٥0 ml of the AB solution with an initial concentration of 30 mg L^{-1} at pH 5.0 and different temperatures ranging from 293 to 318 K. The mixtures were shaken for 24 h then the equilibrium dye concentration was detected for each experiment.

Results and discussion

Characterization

XRD

The structural characterization of the synthesized samples was examined by XRD and the patterns are presented in Fig. 1(a). As shown, all synthesized samples exhibit a broad peak around 2θ of 20° due to the amorphous structure of the gelatin and gelatin/chitosan blends [20]. However, G100 showed a small peak at 2θ = 7.3° which belongs to the crystallites of the ordered triple-helical structure of collagen [21]. This peak appeared with lower intensity in G75 sample but disappeared in the case of G50 and G25 indicating that blending with chitosan restricts the formation of triple-helical structure between gelatin chains. This is due to the extensive intermolecular attraction between -NH_2, -COOH and -OH in gelatin chains with -NH_2 and -OH in chitosan chains which results in a completely amorphous structure [20].

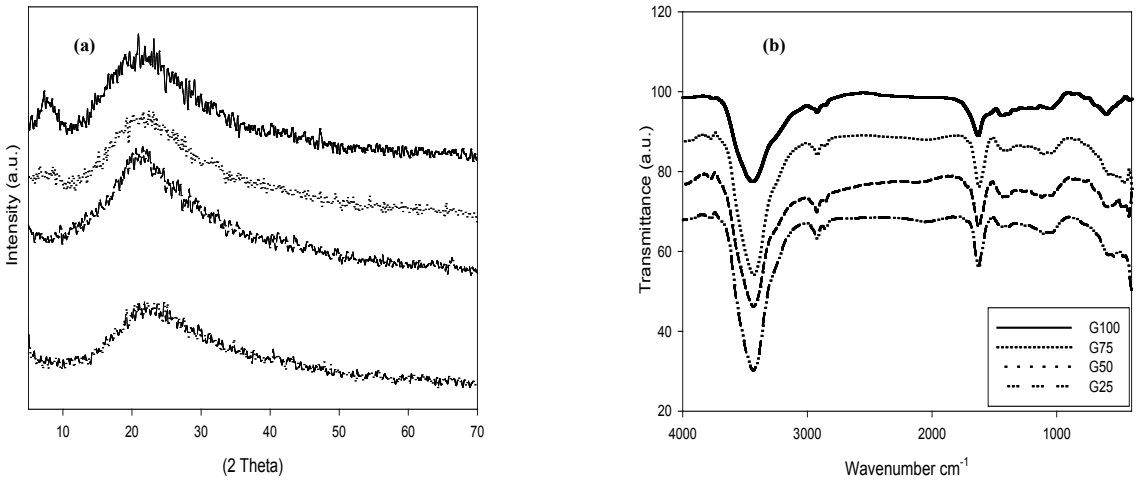

Fig. 1. (a) XRD patterns of the synthesized samples, (b) FT-IR spectra of the synthesized samples.

FT-IR

FTIR spectra for synthesized samples are shown in Fig 1 (b). Absorption peaks around 3440 and 3250 cm^{-1} belong to NH and OH stretching vibration. The absorption peak of NH appeared at 3440 cm^{-1} in G100 but shifted to 3430 cm^{-1} in blends which is attributed to the H bonding between gelatin and chitosan chains [22]. The absorption peaks around 2900 and 2850 are attributed to (CH_2) and C–H stretching vibrations of alkyl groups in gelatin and methylene in chitosan chains. Absorption peaks of amide groups appear around 1640 and 1240 cm^{-1} due to C=O stretching vibrations, C-N stretching vibrations respectively. However, the characteristic peak of N-H bending at 1550 cm^{-1} was not observed in all samples which indicate that NH_2 group of the polymers reacted through Schiff base reaction with the aldehyde group in glutaraldehyde. The absorption peak at 1045 cm^{-1} in all samples is attributed to the reaction between hydroxyl groups (–OH) in polymer chains and (C=O) in glutaraldehyde forming C–O–C–O–C form [23].

Degree of solubility of the synthesized samples in aqueous media

The synthesized samples were stable when soaked in aqueous media (stability was greater than 99.8%) below 40 °C. However, at higher temperatures samples showed a lower degree of stability when soaked in water for 24 h. These results revealed that gelatin was not chemically cross-linked completely where some of the gelatin chains were free to flow out of the polymeric matrix as a result of soaking in hot water for 24 h. As chitosan content increases in the blends, the degree of solubility decreases which is attributed to the lower content of gelatin in this blend. Table 2. shows the degree of solubility (%) for synthesized samples.

pH-responsive equilibrium swelling and point of zero surface charge

The degree of swelling of the adsorbents at different pH values affects their adsorption efficiency. Fig 2 (a) shows the plot of resulted ES values versus pH. As shown in the Fig., G100 showed higher ES than other samples over the whole range of the studied pH values. This is revealed to the higher tendency of chitosan to be cross-linked with gluteraldehyde compared with gelatin [23]. Although a fixed amount of cross-linker is added per gram of polymer, the samples that contain chitosan chains were more cross- linked than G100 sample. In addition, G100 showed the maximum swelling at PH 2 and 3 which is attributed to the protonation of NH_2 groups forming NH_3^+ on the polymeric chains where the repulsion between the positively charged sites enhances the swelling. However, at higher pH values, gelatin chains acquire negative charges due to the ionization of carboxylic groups forming COO^- [24]. The electrostatic attraction between COO^- and NH^{3+} on the polymeric chains acts as extra cross-linking which decreases the swelling [25]. In alkaline medium, all carboxyl groups are ionized forming COO- and the electrostatic anion–anion repulsion slightly enhances the swelling process.

Fig.2 (b) shows the plot of pH_i versus (pH_i–pH_f) as detected from Batch equilibrium method, the point of zero surface charge was found to be 6 for all samples. These results indicate that the net adsorbent surface charge is positive below pH 6 and negative at higher pHs.

Adsorption studies

Effect of pH

The pH of the adsorbate solution influences the adsorption capacity because it controls the charge of the adsorbent surface and the ionization of the functional groups of adsorbents. To study the effect of pH on the adsorption capacity of the synthesized samples, 0.1 g of each adsorbent was immersed in 50 ml of AB solution (30 mg L^{-1}) of definite pH using buffer solutions for 24 h at 20 °C with shaking. Fig.3 illustrates the effect of adsorbate pH on the dye removal (%E). G100 showed the greatest dye removal (%E) at pH 2 and 3 which was attributed to the protonation

TABLE 2. Degree of solubility (%) for synthesized samples.

Sample code	40 °C	50 °C
G100	92.3	86.1
G75	96.6	95.5
G50	98.7	97.5
G25	99.7	98.5

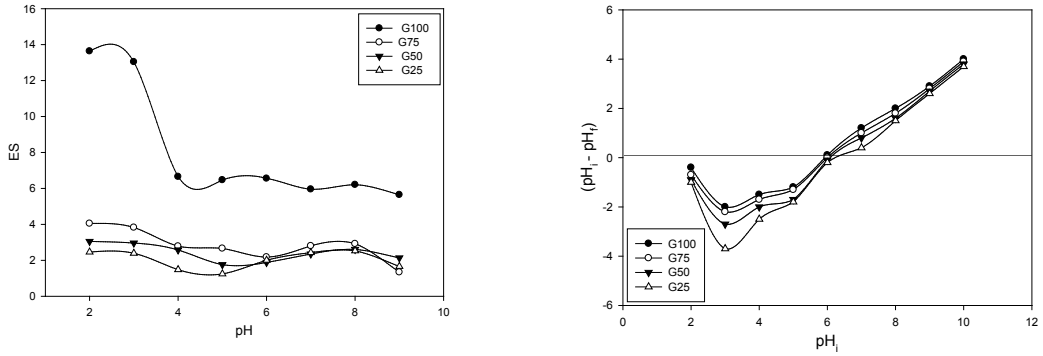

Fig. 2 (a). Effect of pH on the ES for synthesized samples at 20 °C for 24 h, (b) pH_{pzc} for synthesized samples as detected by batch equilibrium method.

of NH_2 groups into NH_3^+ as well as the high ES. However, adsorption (%E) decreases at pH ≥ 4 due to the repulsion between the ionized carboxylic groups and the anionic dye. G75 and G50 showed nearly constant dye removal (%E) over the studied pH range. This was revealed to the amphoteric nature of these polymer blends wherein the acidic medium the surface is positively charged due to the protonation of NH_2 while in the alkaline medium it is negatively charged due to the ionization of carboxylic groups into COO^-. At pH 6, samples showed a slight decrease in the dye removal (%E) where both samples exhibit zero net surface charge at this pH as explored in section 3.3 so they show minimized tendency to the anionic dye [13]. Below pH 6, the samples are positively charged due to the protonation of amine groups [16], so there is an electrostatic attraction between the adsorbent and the anionic dye. Although the samples have negatively charged surface at pH > 6, the dye removal (%E) samples did not decrease which was revealed to the enhanced swelling as a result of anion-anion repulsion between COO^- groups on the polymeric chains. For G25, increasing pH values increase the dye removal (%E) which suggests either a chemical reaction between the dye and chitosan chains or the formation of H bonding between the secondary amine in the dye molecule and $-CH_2-O^-$ which arise on chitosan chain in alkaline medium. Sakkayawong et al. reported that chitosan undergoes both chemical and physical adsorption in alkaline media [26].

Effect of contact time

Fig. 4 shows the dye removal (%E) plotted versus the contact time. In general, the dye removal (%E) attained equilibrium within 6 h of adsorption in all examined temperatures. The dye removal (%E) for G100 sample decreased with increasing temperature while G25 sample showed increasing dye removal (%E) as temperature increases up to 40 °C. All samples showed a steady-state increase in dye removal (E%) during the first 6 h of adsorption then the rates slowed down. This is attributed to the presence of a large number of available active sites on the adsorbent surface at the beginning of the adsorption reaction. As adsorption reaction proceeds, the number of available active sites decreases and concentration of dye solution decreases which decreases the rate of adsorption.

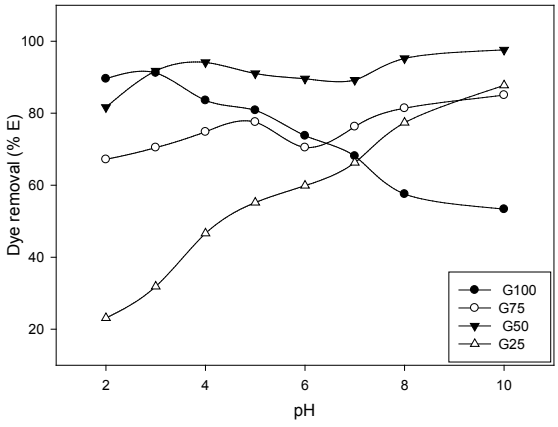

Fig. 3. Effect of pH on dye removal (%E) [adsorbent dose, 0.1 g; AB aq. dye solution, 30 mg L–1at 20 ºC for 24h].

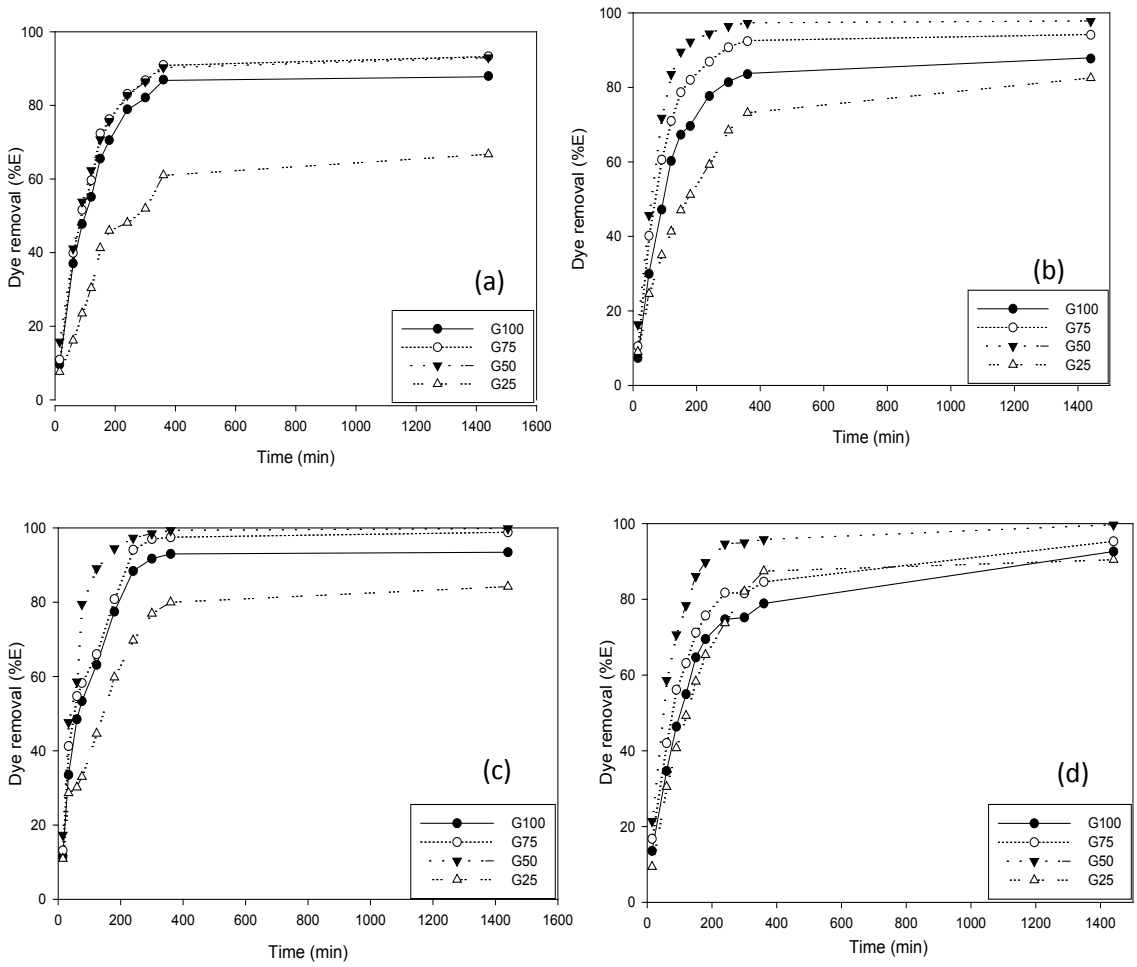

Fig. 4. Effect of contact time on dye removal (% E) at (a) 20 ºC, (b) 30 ºC, (c) 35 ºC, (d) 40 ºC [adsorbent dose, 0.1 g; 50 ml of AB aq. solution, 30 mg L–1 at pH 5 for 24 h].

Effect of initial concentration

To detect the maximum adsorption capacity of adsorbents, it is important to explore the equilibrium adsorption results for various initial adsorbate concentrations. This parameter was investigated as follows: 0.1 g adsorbent was immersed in AB solution of concentration (10, 20, 30, 50 and 100 mg L^{-1}) and pH 5 at 20, 25, 30, 35 ºC for 24 h with shaking. Fig.5 shows that in all studied temperatures, as the initial concentration of AB changed from 10 to 100 (mg L^{-1}), q_e increased. The samples did not exhibit saturation up to initial concentration of 100 mg L^{-1} where increasing the initial concentration of the adsorbate promotes the mass transfer from the solution.

Adsorption kinetics

To investigate the kinetics of the adsorption experiment, the experimental adsorption results were treated by the well-known pseudo–first–order and pseudo–second–order models. The Lagergren's equation of pseudo-first–order model in the linear form is written as:

$$\log (q_e - q_t) = \log q_e - \left(\frac{k_1 t}{2.303}\right) \quad (4)$$

where q_e and q_t are the amount adsorbed (mg g^{-1}) at equilibrium and time t respectively while k_1 (min^{-1}) is the rate constant of the adsorption process. The rate constant k_1 can be detected by plotting log ($q_e - q_t$) versus t where the slope = k_1 /2.303.

The pseudo–second–order equation is characterized by the ability to detect the equilibrium capacity and the initial adsorption rate from the model [27]. The pseudo–second–order equation is expressed as follows:

$$\frac{t}{q_t} = \frac{1}{k_2 q_e^2} + \frac{t}{q_e} \quad (5)$$

where q_e and q_t as described previously and k_2 is the rate constant (g.mg^{-1} min^{-1}).

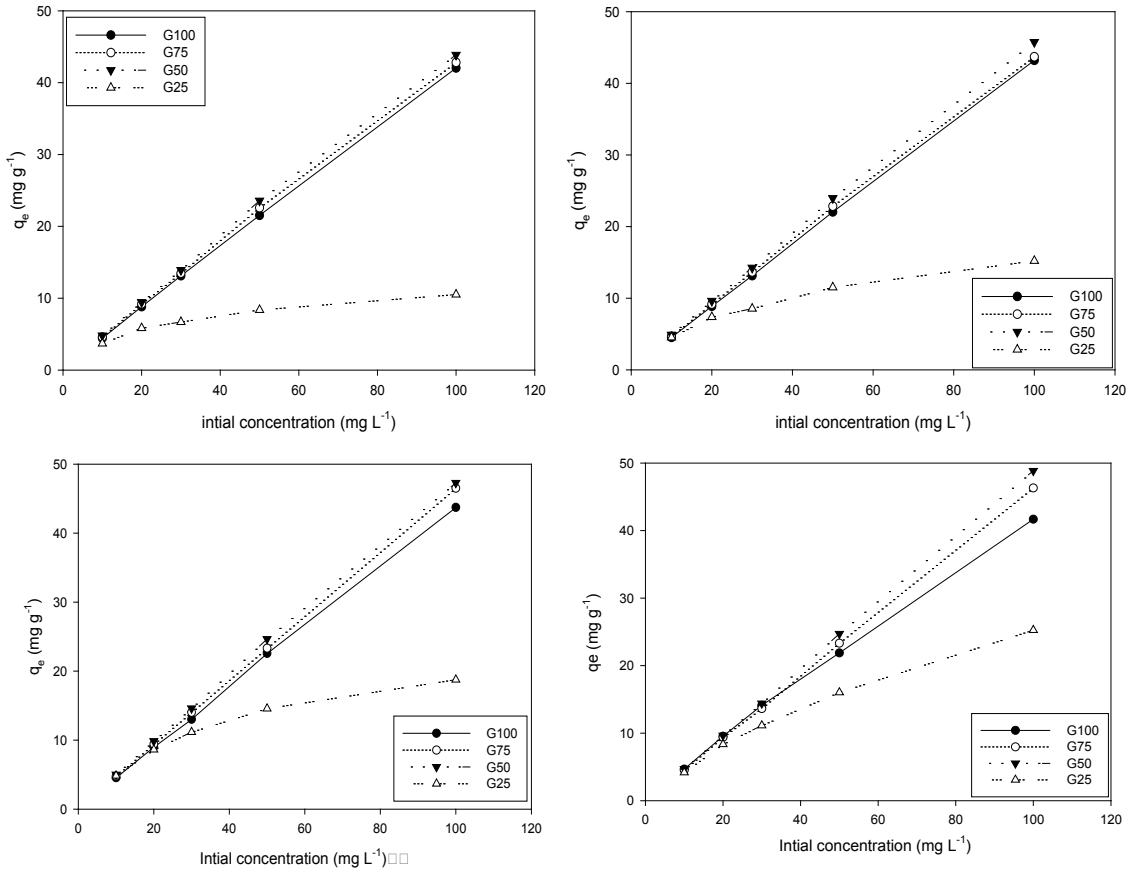

Fig. 5. Effect of initial dye concentration on the adsorption capacity of synthesized samples at (a) 20 ºC, (b) 30 ºC, (c) 35 ºC, (d) 40 ºC [adsorbent dose, 0.1 g l-1 at pH 5 for 24 h].

The plot of t/q_t versus t gives a straight line with slope = $1/q_e$ and the rate constant (k_2) can be detected from the intercept.

Elovich model equation is a rate equation that is applicable for the chemisorption mechanism on energetically heterogeneous solid surface and it can be written as follows [28]:

$$q_t = \frac{1}{b}\ln(ab) + \frac{1}{b}\ln(t) \quad (6)$$

where a is the initial adsorption rate (mg g^{-1} min^{-1}), and the parameter 1/b (mg g^{-1}) is related to the number of available sites for adsorption. If plotting qt versus ln (t) produces a straight line then the experimental results fit this model.

Table 3 illustrates the parameters obtained from the fitting of experimental data with the three models. As shown, the experimental results show the best fitting to pseudo– second–order model with R^2 =1 in most cases. In addition, the value of q_e detected theoretically from the model was close to that detected experimentally. For all samples the Elovich equation did not fit the experimental data at different temperatures as shown by R^2. These results indicate that the adsorption process takes place on an energetically heterogeneous surface. G50 sample showed the greatest value for K_2 in each temperature over the other samples which indicates that G50 exhibits the greatest rate of adsorption. The value of q_e slightly increases as temperature increases up to 308 K but further increase in temperature to 313 K leads to decreasing adsorption capacity. This was attributed to the dissolution of some of gelatin chains from the adsorbent. Similar results were obtained for adsorption of acid red 337 on gelatin/chitosan microspheres [13]. It was noticed that for each adsorbent, as temperature increases the rate constant value increases suggesting the adsorption process is an endothermic process.

The activation energy for the adsorption process is detected using Arrhenius equation as follows:

$$\ln K_2 = \ln A - \frac{E_a}{RT} \quad (7)$$

where K_2 is the rate constant obtained from pseudo-second order model, A the temperature-independent parameter (g mg^{-1} min^{-1}), E_a is the activation energy of the adsorption process (kJ mol^{-1}), R is the universal gas constant 8.314 x 10^{-3} (kJ mol^{-1} K^{-1}) and T is the temperature (K). The activation energy is detected from the slope of the straight line obtained from plotting of ln K_2 versus 1/T. If E_a is less than 40 kJ mol^{-1} then the adsorption is physisorption while E_a > 40 kJ mol^{-1} indicates a chemisorption process [29].

Fig. 6 presents the plot of ln K_2 versus 1/T and Ea values were estimated from the slopes as 13, 16, 30, 48 kJ mol^{-1} for G100, G75, G50 and G25 respectively. According to these values the adsorption is physisorption in nature for all samples except G25. It is noticed that as chitosan content increases in the polymer blend, the activation energy increases. These results suggest that a part of the functional groups on chitosan chains interact chemically with the dye molecules while gelatin chains adsorb the dye molecules through physical electrostatic attraction. These observations suggest that for polymer blends both chemisorption and physisorption mechanisms are included where the chemisorption mechanism is the predominant when chitosan % is greater than gelatin.

Adsorption mechanism

The studied kinetic models cannot propose the mechanism of adsorption process; so, the experimental results were examined using the intra-particle diffusion model to investigate the rate-determining step. This model assumes that the intra-particle diffusion is the rate-determining step and its rate constant can be detected from the equation [30]:

$$q_t = k_i t^{0.5} + C \quad (8)$$

where k_i is the rate constant of the intra-particle diffusion step (mg g^{-1} $min^{-0.5}$) and C (mg g^{-1}) is a parameter indicating the thickness of the boundary layer whereas the numerical value of C increases the boundary layer effect increases. According to Eq.8 if q_t is plotted versus the square root of time ($t^{0.5}$), a straight line passes through the origin is obtained. However, if the intra-particle diffusion is not the only rate-limiting step, the straight line will not pass through the origin. In addition, if two or more intersecting lines are obtained that means two or more steps are controlling the adsorption process[31,32]. Fig. 7 illustrates the fitted experimental results to the intra-particle diffusion model. The results suggest that the intra-particle diffusion step is not the only rate-limiting step and the adsorption process takes place in three steps with decreasing rates. The first step is the fast-surface adsorption followed by the intra-particle diffusion with a slower rate. The last step is equilibrium step where the adsorption slows down due to the low concentration of adsorbate as well as the absence of available sites for adsorption.

TABLE 3. Kinetics parameters for the adsorption of AB (30 mg g^{-1}) at pH 5.0, 20, 30, 35 and 40 °C for 24 h.

Temperature (K)	Adsorbent	qe [experimental] (mg g)	pseudo- first order			pseudo- second order			Elovich's equation		
			q_e (mg g-1)	$K_1 X10^3$ (min^{-1})	R^2	q_e(mg g-1)	K_2 (g.mg^{-1}.min^{-1})	R^2	A (mg g^{-1} min^{-1})	1/b (mg g-1)	R^2
293	G100	13.166	3.020	8.316	0.997	13.868	40.596	0.998	0.434	2.897	0.900
	G75	13.97	3.16	8.68	1.00	14.73	48.21	1.00	0.46	3.07	0.90
	G50	13.92	2.93	8.53	0.99	14.49	59.82	1.00	0.67	2.82	0.89
	G25	9.97	2.81	6.25	0.95	11.17	9.30	0.99	0.19	2.29	0.90
303	G100	13.29	2.86	7.82	0.99	13.878	47.615	0.999	0.531	2.799	0.898
	G75	14.25	3.03	10.00	0.99	14.96	60.85	1.00	0.64	3.06	0.86
	G50	14.67	3.00	13.74	0.98	15.14	108.02	1.00	1.05	2.94	0.78
	G25	10.65	3.17	10.46	0.95	11.42	17.69	1.00	0.31	2.38	0.76
308	G100	13.94	3.50	13.88	0.97	14.68	55.90	1.00	0.560	3.046	0.887
	G75	14.75	3.31	12.27	0.97	15.45	70.63	1.00	0.69	3.08	0.88
	G50	14.90	2.93	14.19	0.99	15.33	122.56	1.00	1.27	2.85	0.79
	G25	12.56	3.08	8.09	0.98	13.54	26.36	1.00	0.33	2.79	0.91
313	G100	12.24	2.86	8.89	0.99	12.85	55.60	1.00	0.517	2.559	0.877
	G75	13.02	2.86	9.61	1.00	13.51	72.67	1.00	0.82	2.51	0.88
	G50	14.57	2.67	11.13	0.98	14.91	129.09	1.00	1.88	2.52	0.79
	G25	13.57	3.36	9.21	0.99	14.56	32.61	0.99	0.35	3.15	0.89

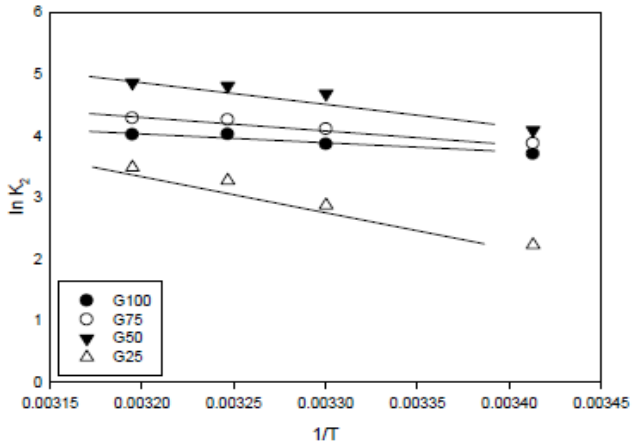

Fig. 6. The plot of Arrhenius equation.

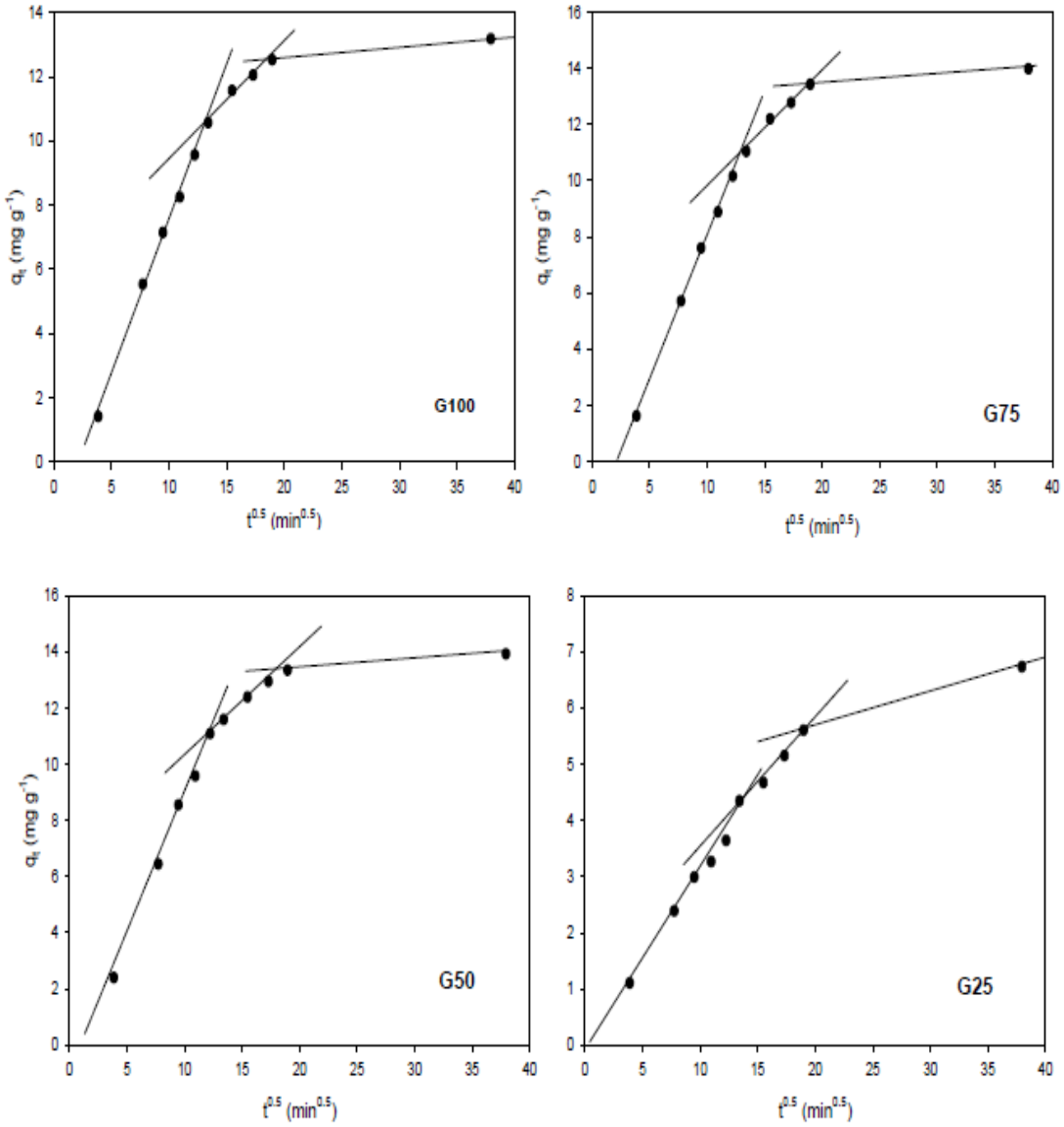

Fig. 7. Intra-particle diffusion plots for adsorption of AB, 30 mg L–1 at pH 5 and 20 ºC for 24 h.

The intra-particle diffusion rate constant k_i was detected as the slope of the second region where the intra-particle diffusion takes place [33]. The values are 0.346, 0.353, 0.367 and 0.704 mg g^{-1} $min^{-0.5}$ for G100, G75, G50 and G25 respectively. These results indicate that as chitosan content increases the rate of intra-particle diffusion step increases.

Adsorption isotherms

The adsorption equilibrium data were examined using the well-known Langmuir, Freundlich and Dubinin–Radushkevich (D-R) isotherm models.

Langmuir isotherm

This model assumes that the adsorbate molecules are arranged on the adsorbent surface as a monolayer where the adsorbent has a definite number of active sites with identical activation energy and the steric hindrance between the adjacent adsorbate particles is neglected [34]. This isotherm is usually fit chemisorption mechanisms and its linear form is written as follows [35]:

$$\frac{C_e}{q_e} = \frac{1}{bQ_e} + \frac{C_e}{Q_e} \quad (9)$$

where C_e is the adsorbate concentration in the solution at equilibrium (mg L^{-1}) and q_e is as mentioned previously. Q_e is the maximum adsorption capacity as detected theoretically (mg g^{-1}) and b is the Langmuir parameter ($L.mg^{-1}$).

Freundlich isotherm

This isotherm proposes a multilayer adsorption mechanism where that the adsorbent has active sites with different adsorption energies [36]. The linear form of this model is expressed as follows:

$$\log q_e = \log k_f + \frac{1}{n} \log C_e \quad (10)$$

where q_e and C_e are mentioned previously, k_f is the Freundlich constant [mg g^{-1} (mg L^{-1})^n] and n is a parameter related to the heterogeneity of the adsorption sites energies (dimensionless). k_f and $1/n$ are detected from the intercept and the slope of the straight line obtained when log q_e is plotted versus log C_e. The slope, $1/n$, takes a value between 0 and 1, where the closer 1/n to zero the more heterogeneous surface is [34].

Dubinin–Radushkevich Isotherm

Dubinin–Radushkevich (D-R) isotherm distinguishes the nature of the adsorption process either physisorption or chemisorption. The linear form of this model is written as follows:

$$\ln q_e = \ln q_{(D-R)} - \beta\varepsilon^2 \quad (11)$$

$$\varepsilon = RT \ln\left(1 + \frac{1}{C_e}\right) \quad (12)$$

$$E = \frac{1}{\sqrt{2\beta}} \quad (13)$$

where q_e and C_e are mentioned previously, $q_{(D-R)}$ is the theoretical capacity in the case of saturation (mg g^{-1}), ε is Polanyi's potential and β is a parameter related to adsorption energy for each mole of the adsorbate (mol^2. kJ^{-2}). R is the universal gas constant (8.314 $X10^{-3}$ kJ K^{-1} mol^{-1}) and T is the absolute temperature (K). E is the mean energy per molecule of adsorbate when it migrates from the solution (infinity) to the solid surface of the adsorbent ($kJ.mol^{-1}$). The numerical value of E indicates the nature of adsorption process where it is less than 8 $kJ.mol^{-1}$ in the case of physisorption process but it is greater than 8 $kJ.mol^{-1}$ in the case of chemisorption process [37]. This model is valid only in a particular range of adsorbate concentrations while higher concentrations show unrealistic behavior [38]. If ln q_e is plotted versus ε^2, a straight line with a slope of –β is obtained, and then E could be detected from Eq.13.

The detected parameters from these models are presented in Table 4. From the values of correlation coefficient R^2 it is obvious that Freundlich isotherm is the more applicable model to describe the adsorption of AB on the synthesized sample. These results suggest that AB is adsorbed as multilayers on the adsorbent surface which supports the physisorption mechanism. The calculated values for 1/n ranges from 0.2 to 0.9 are indicating the heterogeneity of the adsorbent surface. Dubinin–Radushkevich (D-R) isotherm showed satisfying fitting to the experimental data and E values for all synthesized samples were lower than 8 kJ mol^{-1} which indicates that the adsorption process is mostly physisorption in nature.

Thermodynamics studies

Experimental data from temperature-dependent adsorption isotherms at (293, 298, 303 and 308 K) were used to detect the thermodynamics parameters, entropy change (ΔS), enthalpy change (ΔH) and Gibbs energy change (ΔG). The equilibrium constant was detected as follows:

$$K_d = \frac{q_e}{C_e} \quad (14)$$

Then (ΔS), (ΔH) and (ΔG) were detected using the following equation:

$$\Delta G = -RT \ln K_d \quad (15)$$

$$\ln K_d = \frac{\Delta S}{R} - \frac{\Delta H}{RT} \quad (16)$$

where q_e and C_e are previously declared, R is the ideal gas constant (8.314 □ 10^{-3} KJ K^{-1} mol^{-1}) and T is the absolute temperature (K). According to Eq. 15, the plot of ln K_d versus *1/T* produces *a* straight line of a slope $\Delta H/R$ and intercept $\Delta S/R$. The values of R^2 were greater than 0.92 so the detected values for ΔH and ΔS were satisfactory. The estimated thermodynamic parameters are presented in Table 5. ΔH and ΔS showed positive values for all samples which revealed the endothermic nature of the adsorption process as well as the increased randomness as a result of adsorption. The value of ΔS increases in the order G100 < G75< G50 < G25 which indicates that as chitosan content increases in the polymer blend, the disorder resulted from adsorption increases, and the adsorption reaction becomes more favorable. The degree of spontaneity of these reactions where both ΔH and ΔS are positive, depends on the value of the temperature [39]. The calculated ΔG (Eq.15) showed negative values over the studied temperature range for all samples except G25 which exhibited positive values for ΔG up to 298 K. These results indicate that the adsorption of AB on G25 is spontaneous at temperature ≥ 303 K. In general, the degree of spontaneity for the adsorption process increases with increasing the temperature. These observations indicate that the adsorption process is enhanced by increasing the temperature [29].

TABLE 4 . Obtained parameters from Langmuir, Freundlich and Dubinin – Radushkevich (D-R) isotherms.

Temperature	Adsorbent	Langmuir model			Freundlich model			D-R isotherm		
		b	q_{max}	R^2	K_f	1/n	R^2	E	QD-R	R^2
		(L mg^{-1})	(mg g^{-1})		((mg g^{-1})/(mg L^{-1})^n)			(kJ·mol^{-1})	(mg·g^{-1})	
293	G100	0.026	146.471	0.620	1.841	0.864	0.994	1.025	13.984	0.958
	G75	0.059	97.606	0.891	2.156	0.788	0.999	1.170	20.106	0.914
	G50	0.141	72.099	0.891	2.618	0.670	0.994	2.254	17.304	0.944
	G25	0.137	11.257	0.992	1.618	0.299	0.962	0.306	8.812	0.971
298	G100	0.015	277.731	0.330	1.883	0.910	0.995	1.136	13.758	0.957
	G75	0.052	120.463	0.893	2.206	0.827	1.000	1.446	14.415	0.954
	G50	0.189	79.645	0.866	2.959	0.692	0.997	2.652	14.777	0.960
	G25	0.133	16.377	0.978	1.915	0.284	0.991	1.577	8.120	0.968
303	G100	0.009	496.195	0.726	1.903	0.959	0.997	1.130	14.498	0.977
	G75	0.081	116.328	0.859	2.556	0.833	0.987	1.567	18.440	0.977
	G50	0.463	73.453	0.872	3.705	0.642	0.995	3.911	15.975	0.965
	G25	0.185	19.994	0.988	2.152	0.283	0.995	2.523	9.423	0.906
308	G100	0.006	807.813	0.898	1.985	0.969	0.994	1.138	15.968	0.948
	G75	0.009	810.113	0.023	2.294	0.885	0.973	1.147	22.577	0.986
	G50	-0.132	-90.482	0.281	3.205	1.273	0.933	1.652	23.776	0.995
	G25	0.087	30.115	0.972	1.813	0.488	0.973	0.914	11.394	0.993

TABLE 5. Thermodynamic parameters for adsorption of AB (30 mg g^{-1}) at pH 5.0 for 24 h.

T (K)	G100					G75				
	ln Kd	ΔG (J mol^{-1})	ΔH x 10^{-3} (J mol^{-1})	ΔS (J mol^{-1} K^{-1})	R^2	ln Kd	ΔG (J mol^{-1})	ΔH x 10^{-3} (J mol^{-1})	ΔS (J mol^{-1} K^{-1})	R^2
293	1.25	-2830	21.04	81.81	0.920	1.52	-3444	32.27	122.68	0.936
298	1.31	-2963				1.67	-3799			
303	1.44	-3265				2.05	-4648			
313	1.67	-3795				2.11	-4786			
T (K)	G50					G25				
	ln Kd	ΔG (J mol^{-1})	ΔH x 10^{-3} (J mol^{-1})	ΔS (J mol^{-1} K^{-1})	R^2	ln Kd	ΔG (J mol^{-1})	ΔH x 10^{-3} (J mol^{-1})	ΔS (J mol^{-1} K^{-1})	R^2
293	1.86	-4228	56.75	209.70	0.955	-0.90	2039	66.75	220.72	0.968
298	2.35	-5341				-0.40	905			
303	2.83	-6427				0.20	-445			
313	2.96	-6719				0.38	-870			

Conclusions

Chemically cross-linked gelatin and gelatin / chitosan blends were successfully synthesized using glutaraldehyde as a cross-linker. The samples show stability in aqueous media up to 35 ^{o}C but exhibit dissolution at higher temperatures. Adsorption efficiency of the samples is examined using an aqueous solution of aniline blue. Samples exhibit point of zero surface charge around pH 6. Samples attain adsorption equilibrium within 6 h and did not show saturation up to dye concentration of 100 mg L^{-1}. kinetics data fit pseudo second order model. The activation energy values confirmed that the cross-linked gelatin and gelatin/chitosan blends, up to 50% chitosan content, exhibit physisorption process. However, blend with 75% chitosan exhibits higher activation energy as an evidence of chemisorption behavior. Freundlich isotherm showed a better fit than the Langmuir isotherm, thus, indicating a multilayer adsorption of the dye on the adsorbent surface. Thermodynamics studies indicate that the adsorption is endothermic, spontaneous and leads to a higher entropy. These results suggest that the gelatin/chitosan blend of 50 wt.% gelatin and 50 wt.% chitosan is a promising biodegradable eco-friendly adsorbent that could be used for removal of anionic dyes from wastewater.

Acknowledgements

The authors are grateful to the National Research Centre for the equipment facilities.

Conflict of Interest: The authors declare that they have no conflict of interest.

Financial funding and support: The authors declare that there are no sources of financial funding and support.

References

1. Hassaan MA, Nemr A El Health and Environmental Impacts of Dyes: Mini Review *Am J Environ Sci Eng.* **1**, 64-67. https://doi.org/10.11648/j.ajese.20170103.11 (2017).

2. Rangabhashiyam S, Anu N, Selvaraju N Sequestration of dye from textile industry wastewater using agricultural waste products as adsorbents *J Environ Chem Eng.* **1,** 629-641 doi:10.1016/j.jece.2013.07.014 (2013).

3. Hidalgo AM, León G, Gómez M, Murcia MD, Gómez E, Gómez JL Modeling of Aniline Removal by Reverse Osmosis Using Different Membranes *Chem Eng Technol.* **34,** 1753-1759. https://doi.org/10.1002/ceat.201000510 (2011).

4. Verma AK, Dash RR, Bhunia P A review on chemical coagulation/flocculation technologies for removal of colour from textile wastewaters *J Environ Manage* **93,** 154-168 (2012).

5. Azizi E, Ghayebzadeh M, Beikmohammadi M, Sharafi K Oxidation of aniline with photo-Fenton advanced oxidation process from aqueous solutions in batch reactor *Tech J Eng Appl Sci* **5**, 12-16 (2015).

6. Awin LA, A. El-Rais M, M. Etorki A, Mohamed NA, Makhlof WA Removal of Aniline Blue from Aqueous Solutions Using $Ce_{1-x}Bi_xCrO_3$ (x = 0, 0.5, 1) *Open J Inorg Non-metallic Mater* **08** 1–10 https://doi.org/10.4236/ojinm. 2018.81001 (2018).

7. Shao L, Cheng XQ, Liu Y, Quan S, Ma J, Zhao SZ, Wang KY Newly developed nanofiltration (NF) composite membranes by interfacial polymerization for Safranin O and Aniline blue removal. *J Memb Sci.* **430,** 96–105. https://doi.org/10.1016/j.memsci.2012.12.005 (2013).

8. You X, Li E, Liu J, Li S Using natural biomacromolecules for adsorptive and enzymatic removal of aniline blue from water. *Molecules* **23,** 1–14. https://doi.org/10.3390/molecules 23071606 (2018).

9. Moawed EA, Abulkibash AB, El-Shahat MF Synthesis and characterization of iodo polyurethane foam and its application in removing of aniline blue and crystal violet from laundry wastewater. *J. Taibah Univ Sci.* **9,** 80–88. https://doi.org/10.1016/j.jtusci.2014.07.003 (2014).

10. Gupta VK, Carrott PJM, Ribeiro Carrott MML, Suhas Low-Cost adsorbents: Growing approach to wastewater treatmenta review. *Crit. Rev. Environ. Sci. Technol.* **39**, 783-842 doi:10.1080/10643380801977610 (2009).

11. Saber-Samandari S, Saber-Samandari S, Joneidi-Yekta H, Mohseni M Adsorption of anionic and cationic dyes from aqueous solution using gelatin-based magnetic nanocomposite beads comprising carboxylic acid functionalized carbon nanotube. *Chem Eng J*. **308,** 1133-1144 https://doi.org/10.1016/j.cej.2016.10.017 (2017).

12. He B, Wang X, Xue H, Hao X Preparation and Adsorption Properties of Gelatin Microspheres for Cationic Dye. *Adv Mater Res.* 415-417 1794-1798. https://doi.org/10.4028/www.scientific.net/AMR.415-417.1794 (2011).

13. He B, Xue H Adsorption behaviors of acid dye by amphoteric chitosan/ gelatin composite microspheres. *Water Qual Res J Canada*. **50** 314-325 https://doi.org/10.2166/wqrjc. 2015.001(2015).

14. Li W, Ma Q, Bai Y, Xu D, Wu M, Ma H Facile fabrication of gelatin/bentonite composite beads for tunable removal of anionic and cationic dyes. *Chem Eng Res Des.* **134,** 336-346 https://doi.org/10.1016/j.cherd. 2018.04.016 (2018).

15. Kavianinia I, Plieger PG, Kandile NG, Harding DR Preparation and characterization of chitosan films, cross-linked with symmetric aromatic dianhydrides

to achieve enhanced thermal properties. *Polym Int*. **64,** 556-562 https://doi.org/10.1002/pi.4835 (2014).

16. Desbrières J, Guibal E Chitosan for wastewater treatment. *Polym. Int*. **67,** 7-14 (2017).

17. Dotto GL, Moura JM, Cadaval TRS, Pinto LAA Application of chitosan films for the removal of food dyes from aqueous solutions by adsorption. *Chem Eng J*. **214,** 8-16 https://doi.org/10.1016/j.cej. 2012.10.027 (2013).

18. Wang R, Jiang X, He A, Xiang T, Zhao C An in situ cross-linking approach towards chitosan-based semi-IPN hybrid particles for versatile adsorptions of toxins. *RSC Adv.* **5,** 51631-51641. https://doi.org/10.1039/c5ra04638f (2015).

19. Mohamed SK, Hegazy SH, Abdelwahab NA, Ramadan AM Coupled adsorption-photocatalytic degradation of crystal violet under sunlight using chemically synthesized grafted sodium alginate/ZnO/graphene oxide composite. *Int J Biol Macromol* **108,** 1185-1198 https://doi.org/10.1016/j.ijbiomac.2017.11.028 (2017).

20. Chen Z, Mo X, He C, Wang H Intermolecular interactions in electrospun collagen-chitosan complex nanofibers. Carbohydr Polym. https://doi.org/10.1016/j.carbpol. 2007.09.018 (2008).

21. Pereda M, Ponce AG, Marcovich NE, Ruseckaite RA, Martucci JF. Chitosan-gelatin composites and bi-layer films with potential antimicrobial activity. *Food Hydrocoll*. **25,** 1372-1381https://doi.org/10.1016/j.foodhyd. 2011.01.001 (2011).

22. Subramanian K, Indumathi S, Vijayakumar V Fabrication and evaluation of chitosan-gelatin composite film as a drug carrier for in vitro transdermal delivery. *Int. J. Pharm. Sci. Res*. **5**, 438-447. https://doi.org/10.13040/IJPSR.0975-8232. **5**(2), 438-47 (2014).

23. Qian YF, Zhang KH, Chen F, Ke QF, Mo XM Cross-linking of gelatin and chitosan complex nanofibers for tissue-engineering scaffolds. *J.Biomater Sci. Polym. Ed* **22**, 1099-1113 https://doi.org/10.1163/092050610X499447 (2011).

24. Mao J, Kondu S, Ji HF, McShane MJ. Study of the near-neutral pH-sensitivity of chitosan/gelatin hydrogels by turbidimetry and microcantilever deflection *Biotechnol Bioeng*. **95,** 333-341https://doi.org/10.1002/bit.20755 (2006).

25. Bukhari SMH, Khan S, Rehanullah M, Ranjha NM Synthesis and Characterization of Chemically Cross-Linked Acrylic Acid/Gelatin Hydrogels: Effect of pH and Composition on Swelling and Drug Release. *Int. J. Polym. Sci.* **2015** 1-15https://doi.org/10.1155/2015/187961 (2015).

26. Sakkayawong N, Thiravetyan P, Nakbanpote W Adsorption mechanism of synthetic reactive dye wastewater by *J. Text. Color. Polym. Sci.* **16***,* No. 2 (2019) chitosan. *J Colloid Interface Sci* **286**, 36-42 https://doi.org/10.1016/j.jcis.2005.01.020 (2005).

27. Ho YS. Review of second-order models for adsorption systems. *J. Hazard Mater* **136**, 681-689 https://doi.org/10.1016/j.jhazmat. 2005.12.043 (2006).

28. de Oliveira Brito SM, Andrade HMC, Soares LF, de Azevedo RP Brazil nut shells as a new biosorbent to remove methylene blue and indigo carmine from aqueous solutions *J Hazard Mater* **174,** 84-92 https://doi.org/10.1016/j.jhazmat.2009.09.020 (2010).

29. Boparai HK, Joseph M, O'Carroll DM Kinetics and thermodynamics of cadmium ion removal by adsorption onto nano zerovalent iron particles *J Hazard Mater* **186**, 458-465 https://doi.org/10.1016/j.jhazmat.2010.11.029 (2011).

30. W. J. Weber JCM Kinetics of adsorption on carbon from solution *J Sanit Eng Div*, *Am Soc Civ Eng* **89**, 31-60 (1963).

31. Yakout SM, Elsherif E Batch kinetics, isotherm and thermodynamic studies of adsorption of strontium from aqueous solutions onto low cost rice-straw based carbons *Carbon - Sci Technol* **3**, 144–153. https://doi.org/10.1080/07352680590910410 (2010).

32. Wu FC, Tseng RL, Juang RS. Comparative adsorption of metal and dye on flake- and bead-types of chitosans prepared from fishery wastes *J Hazard Mater* **73**, 63-75https://doi.org/10.1016/S0304-3894(99)00168-5 (2000).

33. Fierro V, Torné-Fernández V, Montané D, Celzard A. Adsorption of phenol onto activated carbons having different textural and surface properties *Microporous Mesoporous Mater* **111**, 276-284 https://doi.org/10.1016/j.micromeso.2007.08.002 (2008).

34. K.Y. Foo BHH Insights into the modeling of adsorption isotherm systems *Chem Eng J*. **156**, 2–10. https://doi.org/10.1016/j.cej.2009.09.013 (2010).

35. Da A. Adsorption from theory to practice. *Adv Colloid Interface Sci* **93**, 135–224 (2001).

36. Freundlich H. Ueber die Adsorption in Loesungen. H Z *Phys Chem* **57**, 385-470 (1907).

37. Omnia ALI, Mohamed S. Adsorption of copper ions and alizarin red S from aqueous solutions onto a polymeric nanocomposite in single and binary systems. *Turkish J Chem* **41**, 967-986 https://doi.org/10.3906/kim-1703-72 (2017).

38. Ayawei N, Ebelegi AN, Wankasi D. Modelling and Interpretation of Adsorption Isotherms. *J Chem* **2017** 1-11 doi:10.1155/2017/3039817 (2017).

39. Whitten, K. W.; Gailey, K. D., Davis RE General Chemistry, 4th ed. Saunders College Publishing, New York, NY, USA (1992).

Received 16/07/2019
Accepted 25/07/2019

الدراسة الحركية والديناميكا الحرارية لامتزاز صبغة الأنيلين الزرقاء على مخلوط بوليمر مترابط من الجيلاتين/كيتوزان

على عكاشة [١]* ، حسام صبحى غنيم [٢] ، عيد خليل [٢] ، سحر كمال محمد [٢]
[١] قسم الطيف ، شعبة الفيزياء، المركز القومى للبحوث ، ٣٣ شارع البحوث ، الدقى - جيزه ، صندوق بريد ١٢٦٢٢ و [٢] قسم الكيمياء ، كلية العلوم ، جامعة حلوان ، عين حلوان ، القاهرة ، ١١٧٩٥ ، مصر

تم بنجاح صناعه غشاء من الجيلاتين والكيتوزان المتشابك باستخدام الجلوترالدهيد , العينات المصنعه تم قياسها باستخدام اطياف الاشعه تحت الحمراء وحيود اشعه اكس و الذوبانيه في وسط مائي وزياده الحجم استجابه للرقم الهيدروجيني ونقطه تعادل شحنه السطح . كما تم دراسه كفاءه الامتزاز العينات للانلين الازرق في وسط مائي وكذلك دراسه متغيرات مخنلفه مثل الرقم الهيدروجيني و التركيز الاولي للصبغه و وقت التلامس ودرجه الحراه واختبارهم و قد اظهرت دراسات الحركه ان الامتزاز افضل وصف له باستخدام قانون زيدو الثاني ونتائج اتزان الامتزاز جائت متوافقه مع نموذج فرندليش كماتوافقت البيانات العمليه مع نموذج دبنن رديفيتش وهذا يشير الي غالبيه الامتزاز فيزيائي و كانت اقصي ازاله للصبغه تحقق باستخام ١:١ جيلاتين/ كيتوزان عند رقم هيدروجيني ٥ ودرجه حراره ٣٥ درجه سيلزسه وكانت الازاله للصيغه بنسيه ٩٩,٨ ٪. كما ان طاقه التفعيل لعمليه الامتزاز زادت مع زياده نسبه الكيتوزان وهذا يشير الي سلوك امتزاز كيميائي و كذلك الدراسات الديناميكية الحرارية وضحت ان عمليه الامتزاز تلقائيه وماصه لحراره وتؤدي الي زياده العشوائيه.